Time-resolved solvation of alkali ions in superfluid helium nanodroplets

Ernesto García-Alfonso, Manuel Barranco, Nadine Halberstadt, Martí Pi

Time-resolved solvation of alkali ions in superfluid helium nanodroplets

Ernesto García-Alfonso,[1] Manuel Barranco,[2,3] Nadine Halberstadt*,[1] and Martí Pi[2,3]
[1)]*Laboratoire Collisions, Agrégats, Réactivité (LCAR), Université de Toulouse, CNRS, 31062, Toulouse, France*
[2)]*Departament FQA, Facultat de Física, Universitat de Barcelona, Av. Diagonal 645, 08028 Barcelona, Spain.*
[3)]*Institute of Nanoscience and Nanotechnology (IN2UB), Universitat de Barcelona, Barcelona, Spain.*

(*Electronic mail: nadine.halberstadt@irsamc.ups-tlse.fr)

(Dated: 28 March 2024)

The sinking of alkali cations in superfluid ^{4}He nanodroplets is investigated theoretically using liquid ^{4}He time-dependent density functional theory at zero temperature. The simulations illustrate the dynamics of the build up of the first solvation shell around the ions. The number of helium atoms in this shell is found to linearly increase with time during the first stages of the dynamics. This points to a Poissonian capture process, as concluded in the work of Albrechtsen et al. on the primary steps of Na^+ solvation in helium droplets [S. H. Albrechtsen et al., Nature **623**, 319 (2023)]. The energy dissipation rate by helium atom ejection is found to be quite similar between all alkalis, the main difference being a larger energy dissipated per atom for the lighter alkalis at the beginning of the dynamics. Also, the number of helium atoms in the first solvation shell is found to be lower at the end of the dynamics than at equilibrium for both Li^+ and Na^+, pointing to a kinetic rather than thermodynamical control of the snowball size for small and strongly attractive ions.

I. INTRODUCTION

The study of ion motion in liquid helium has been used to investigate some of the peculiar properties of this unique quantum fluid. In particular, many experimental and theoretical studies have aimed at characterizing ion mobilities inside superfluid helium by drifting the ions through the liquid by means of an external electric field and measuring their time of flight spectrum, see e.g. Refs. 1–3 and references therein. Most of these experiments were designed to study the response of bulk superfluid helium at the atomic scale.

The interaction of a He atom with a cation is very strong compared to that with a neutral atom. This leads to the appearance of a high density –some times solid-like– solvation shell around the cation: the so-called "snowball". Often, several additional high density solvation shells can be distinguished. For very strong interactions, the first shell is nearly isolated, hampering bosonic exchanges with the rest of the superfluid. Note that the term of "snowball" can have different meanings in the literature, so that it is somewhat ill-defined.[4] Here it will refer to the first, high density shell of helium appearing around the ion.

Studies of ions in helium drops are less common. They have been comprehensively reviewed in a recent paper.[4] Cations, like most neutral impurities, reside in the bulk of the drops. This leads to an interesting effect in the case of alkali (Ak) atoms ionization. Ak atoms have the peculiar property of remaining outside, in a dimple of the droplet surface. Upon Ak ionization, the resulting Ak^+ ion sinks into the droplet.[5] At variance with the situation in bulk liquid He, this motion does not require the application of any external electric field to proceed. It has been found that cation sinking can yield quantized vortex rings, as seen for the alkaline-earth Ba^+ ions[6] (Ba atoms also reside on the drop surface), or vortex loops nucleation as in the case of Rb^+ and Cs^+ cations.[5]

The sinking of Ba^+ had been monitored in real time through its absorption spectrum. The latter reflected the location of Ba^+: initially at the droplet surface, it gradually moved inside, where the spectrum characteristics were very similar to the ones in bulk liquid helium.[7] The experiment was accurately reproduced in a ^{4}He-TDDFT analysis.[6] No similar study of the time-resolved absorption spectrum has been carried out for other sinking cations.

An extensive experimental study on the formation and stability of snowball complexes upon photoionization of Na, K, Rb and Cs alkali metal clusters on He nanodroplets has been conducted by Müller et al.[8] using femtosecond laser pulses (multiphoton ionization). Relevant theoretical activity on ions in He drops carried out before 2009 is summarized in Refs. 8 and 9. As already mentioned, alkali atoms are weakly bound to the helium droplet surface:[10] this is due to the extremely weak attractive interaction between Ak and He atoms. Above-threshold laser ionization then leads to massive He atoms evaporation as well as to the expulsion of the ionized dopant, which carries along He atoms forming a snowball structure. The $Ak^+@He_n$ ion abundances in experimental mass spectra are compared to theoretical predictions and are found to agree on the first He shell closure for Rb and Cs snowballs within experimental error. The number of He atoms found for the Rb^+ and Cs^+ snowballs is of 14 and 16, respectively.[8] No differential mass spectrum of snowballs similar to those of Rb^+ and Cs^+ are provided for Na^+ and K^+. In contrast to the heavier Rb and Cs alkali metals, the lighter Na and K species show only very limited snowball progressions in these experiments ($Ak^+@^4He_n$ complexes with $n > 8$ were not observed), and the completion of the first solvation shell is not achieved.

The most recent experimental results are from Scheier's group and coworkers, see especially Refs. 4 and 11. In particular, high-resolution mass spectra experiments conducted on $Na^+@^4He_n$ and $K^+@^4He_n$ complexes formed by electron ionization of doped He droplets[11] gave a snowball size slightly

smaller than the calculated one.

A related experimental work has been conducted by Theisen et al. on the sinking of Rb^+ ions[12] and Cs^+ ions.[13] The Ak atom was excited to the $n\,^2P_{1/2}$ ($^2\Pi_{1/2}$) state (n=5 or 6 for Rb or Cs, respectively), and remained on the droplet surface for a time much longer than needed for the droplet to relax around the excited Ak atom. Subsequently, the excited Ak atom was ionized and eventually the Ak^+ ion sank into the droplet. The size of the snowball was not determined.

In a recent experiment, Albrechtsen et al.[14] have been able to unveil the primary steps of ion solvation in helium droplets. This is a remarkable achievement, all the more so considering the recent quote from Markus:[15] "It is impossible to follow by measurements an actual experimental process of the transfer of a single ion from its isolated state in the gas phase to its fully solvated state in a solution. Such a process, however, may be dealt with as a thought process and theoretical considerations may be applied to it". To accomplish this goal, a He nanodroplet doped with a Xe atom inside and a Na atom on the surface was interrogated in a laser pump-probe experiment. The pump pulse ionized the Na atom, thereby initiating the ion solvation process. After a variable time delay, the probe pulse ionized the Xe atom, triggering Coulomb repulsion between the Xe^+ and Na^+ ions. This led to the ejection of Na^+ along with a number n of He atoms. The resulting $Na^+@^4He_n$ complexes were detected and characterized by velocity map imaging. By carefully analyzing the $Na^+@^4He_n$ ion yields as a function of time delay, the authors concluded that the process was Poissonian up to n =5: the first He atoms attached to the Na^+ ion independently of each other with a constant time rate, as shown by the linear time-dependence of the probability distribution peaks $n(t) = At$. This was confirmed by a theoretical simulation based on the ^{4}He-TDDFT approach included in the same publication.

In this work, we extend the theoretical part of the study on Ak^+ cation sinking carried out for Na^+ in Ref. 14, as well as the theoretical study on Rb^+ and Cs^+,[5] to the whole series of alkali atoms, studied under the same conditions. Special attention is paid to the first picoseconds of the process and to determining how the first solvation shell is being filled. To this end, we apply the density functional theory approach for superfluid helium at zero temperature (^{4}He-TDDFT approach, thoroughly exposed in Ref. 16) to a larger, more realistic He droplet made of 2000 He atoms, using a more accurate version of the computing codes.[17]

This work is organized as follows. The ^{4}He-DFT method is briefly described in Sec. II. We present the results in Sec. III, and a Summary is given in Sec. IV. We also provide in the supplementary material movies illustrating the real-time simulations of the sinking of Ak^+ ions addressed in this work. This multimedia material helps capture physical details that would be difficult to present and thoroughly describe in the main text.

II. THE ^{4}HE-DFT APPROACH

The helium density functional (^{4}He-DFT) method and its time-dependent version (^{4}He-TDDFT) have proven to be very powerful numerical tools to investigate superfluid ^{4}He droplets. They derive from a phenomenological approach and constitute a good compromise between accuracy and feasibility. The parameters of the functional have been adjusted to reproduce various properties of bulk superfluid helium such as its equilibrium density, energy per atom and compressibility, as well as the main features of the dispersion relation of its elementary excitations.[18] A detailed description of the method can be found in Refs. 16, 18–20. In this work we have treated Ak impurities as an external field in the statics calculations carried out to obtain the $Ak@He_{2000}$ equilibrium configurations, and Ak^+ ions as classical particles in the dynamics simulations of Ak^+ sinking inside a He_{2000} droplet.[16]

A. Statics

Within the ^{4}He-DFT approach at zero temperature, the energy of a N-atom helium droplet ^4He_N doped with an Ak atom, taken as an external field, is written as a functional of the ^{4}He atom density $\rho(\mathbf{r})$ as

$$E[\Psi] = \int d\mathbf{r}\,\frac{\hbar^2}{2m_{\rm He}}|\nabla\Psi|^2 + \int d\mathbf{r}\,\mathscr{E}_c(\rho) + \int d\mathbf{r}\,\mathscr{V}_{\rm He-Ak}(|\mathbf{r}-\mathbf{r}_{\rm Ak}|)\,\rho(\mathbf{r})\,, \tag{1}$$

where the first term is the kinetic energy of the superfluid, $m_{\rm He}$ is the mass of the ^{4}He atom, and $\Psi(\mathbf{r})$ is the effective wave function (or order parameter) of the superfluid such that $\rho(\mathbf{r}) = |\Psi(\mathbf{r})|^2$ with $\int d\mathbf{r}|\Psi(\mathbf{r})|^2 = N$. The functional $\mathscr{E}_c(\rho)$ we have used contains the He-He interaction term within the Hartree approximation and additional terms describing nonlocal correlation effects.[21] It is a modification of the Orsay-Trento functional[18] which makes it stable even in the presence of very attractive impurities. The interaction of one single He atom with the Ak impurity is represented by the pair potential $\mathscr{V}_{\rm He-Ak}(|\mathbf{r}-\mathbf{r}_{\rm Ak}|)$ taken from Patil.[22] In the calculations involving Ak^+ ions, we have used the $\mathscr{V}_{\rm He-Ak^+}(|\mathbf{r}-\mathbf{r}_{\rm Ak^+}|)$ pair potentials by Koutselos *et al.*[23] Although there are more recent potentials, the ones by Koutselos et al. have been chosen in order to keep a consistent level of accuracy for all alkali ions.

The droplet equilibrium configuration is obtained by solving the Euler-Lagrange (EL) equation arising from functional variation of Eq. (1)

$$\left\{-\frac{\hbar^2}{2m_{\rm He}}\nabla^2 + \frac{\delta\mathscr{E}_c}{\delta\rho} + \mathscr{V}_{\rm He-Ak}(|\mathbf{r}-\mathbf{r}_{\rm Ak}|)\right\}\Psi \equiv \mathscr{H}[\rho]\,\Psi = \mu\Psi\,, \tag{2}$$

where μ is the ^{4}He chemical potential corresponding to the number of He atoms in the droplet ($N = 2000$ in this work, corresponding to a droplet of $R = 28$ Å radius[19]), and $\mathscr{H}$ is

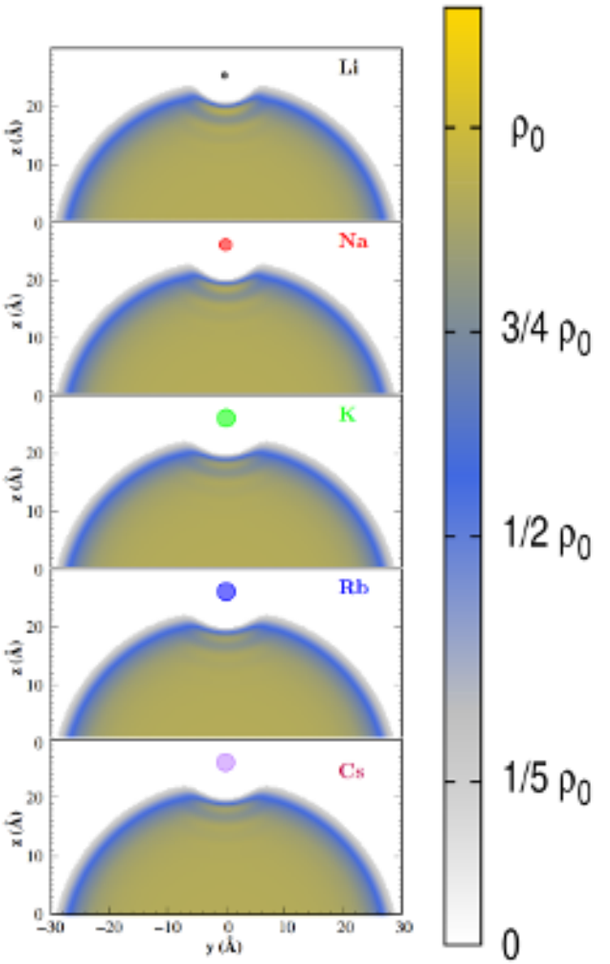

FIG. 1. Equilibrium configuration of Ak@^{4}He$_{2000}$ droplets (two-dimensional cuts). The density scale on the right is given in units of ρ_0, the bulk superfluid helium density at zero temperature and pressure ($\rho_0 = 0.0218$ Å^{-3}). The sharp density radius of He$_{2000}$ is 28.0 Å.

the DFT Hamiltonian

$$\mathscr{H} = -\frac{\hbar^2}{2m_{\rm He}}\nabla^2 + \frac{\delta \mathscr{E}_c}{\delta \rho(\mathbf{r})} + \mathscr{V}_{\rm He-Ak}(|\mathbf{r}-\mathbf{r}_{\rm Ak}|) \qquad (3)$$

The EL equation has been solved by a relaxation (imaginary time) method using the ^{4}He-DFT BCN-TLS computing package,[17] see Refs. 16 and 20 and references therein for additional details. We work in Cartesian coordinates, with the effective wave function $\Psi(\mathbf{r},t)$ defined at the nodes of a 3D grid inside a calculation box discretized using a 0.3 Å space step. Periodic boundary conditions (PBC) are imposed which allow to use the Fast Fourier Transform[24] to efficiently compute the convolutions needed to obtain the DFT mean field $\mathscr{H}[\rho]$. The differential operators in $\mathscr{H}[\rho]$ are approximated by 13-point formulas.

B. Dynamics

The dynamics is triggered by substituting the Ak atom by its ion Ak$^+$. Treating the Ak$^+$ ions as classical particles, the total energy of the system can be written as

$$E[\Psi,\mathbf{r}_{Ak^+}] = \int d\mathbf{r}\,\frac{\hbar^2}{2m_{\rm He}}|\nabla\Psi|^2 + \int d\mathbf{r}\,\mathscr{E}_c(\rho) \qquad (4)$$
$$+ \int d\mathbf{r}\,\rho(\mathbf{r})\,\mathscr{V}_{\rm He-Ak^+}(|\mathbf{r}-\mathbf{r}_{\rm Ak^+}|) + \frac{1}{2}m_{Ak^+}\dot{\mathbf{r}}^2_{Ak^+}\,.$$

The equations describing the dynamics of the system are obtained by minimizing the action[25]

$$\mathscr{A}[\Psi,\mathbf{r}_{\rm Ak^+}] = \int dt\left\{ i\hbar\int d\mathbf{r}\,\Psi^*(\mathbf{r},t)\frac{\partial}{\partial t}\Psi(\mathbf{r},t)\right.$$
$$\left. + m_{\rm Ak^+}\dot{\mathbf{r}}^2_{\rm Ak^+} - E[\Psi,\mathbf{r}_{\rm Ak^+}]\right\}. \qquad (5)$$

Variation of $\mathscr{A}$ with respect to Ψ^* and $\mathbf{r}_{\rm Ak^+}$ yields

$$i\hbar\frac{\partial}{\partial t}\Psi = \left\{-\frac{\hbar^2}{2m_{\rm He}}\nabla^2 + \frac{\delta\mathscr{E}_c}{\delta\rho(\mathbf{r})} + V_{\rm Ak^+He}(|\mathbf{r}-\mathbf{r}_{\rm Ak^+}|)\right\}\Psi$$
$$m_{\rm Ak^+}\ddot{\mathbf{r}}_{\rm Ak^+} = -\int d\mathbf{r}\,V_{\rm Ak^+He}(|\mathbf{r}-\mathbf{r}_{\rm Ak^+}|)\nabla\rho(\mathbf{r})\,, \qquad (6)$$

where the time dependence of the variables has been omitted for clarity. Initial values for the $\{\mathbf{r}_{Ak^+},\dot{\mathbf{r}}_{Ak^+}\}$ variables and the effective wave function $\Psi(\mathbf{r})$ have to be specified. $\Psi(\mathbf{r})$ is taken as the effective wave function corresponding to the equilibrium configuration of Ak@He$_{2000}$, the ion position $\mathbf{r}_{Ak^+}$ as the equilibrium position of neutral Ak in the dimple, and the ion velocity $\dot{\mathbf{r}}_{Ak^+}$ is set to zero.

Equations (6) have been solved using the same simulation box and space step as in the statics. They have been numerically integrated using a Hamming predictor-modifier-corrector algorithm[26] initiated by a fourth-order Runge-Kutta-Gill algorithm[26] implemented in the ^{4}He-DFT BCN-TLS computing package. We have employed a time-step of 0.05 fs except in the case of Li$^+$, where a time step of 0.01 fs has been needed to keep the simulation stable.

Due to the large energy available in the sinking process, very energetic excitations are expected to be produced in the droplet, such as, e.g., phonons, rotons and ripplons. Eventually, this energy is dissipated by He atom ejection. These atoms reach the simulation box boundaries and re-enter the box from the opposite side due to the imposed PBC, interfering with the droplet in an unphysical and unpredictable way. In order to avoid this, an absorption potential is added inside a buffer located near the borders of the simulation box and gradually drives to zero the density corresponding to the evaporated He atoms.[27]

III. RESULTS

A. Statics

Figure 1 shows the equilibrium configuration for each Ak atom in a ^{4}He$_{2000}$ droplet, which is the starting configuration for the sinking dynamics. The dimple in which the Ak

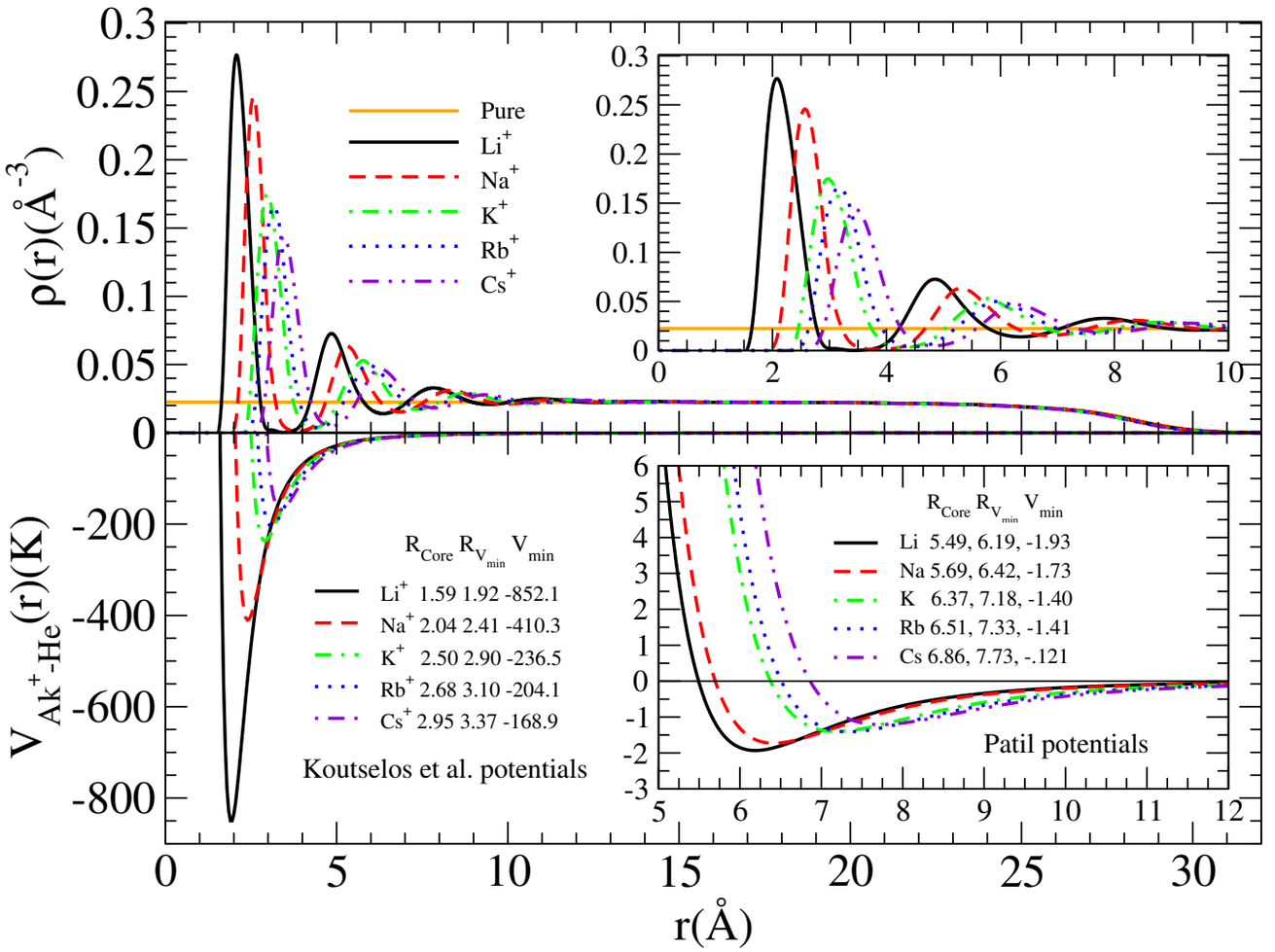

FIG. 2. Top: Spherically averaged helium density profiles of the equilibrium configuration of $Ak^+@^4He_{2000}$ droplets as a function of the distance r to the cation, located at the droplet center. Also shown is the density profile of the pure $^4He_{2000}$ (orange solid line). The insert zooms in on the density profiles in the region $r \leq 10$ Å. Bottom: Ak^+-He pair potentials.[23] The insert displays the corresponding neutral Ak-He pair potentials.[22]

	S_{Ak} (K)	S_{Ak^+} (K)	E_{sink} (K)	r_1 (Å)
Li	-10.1	-7188.9	7007.7	3.5
Na	-9.6	-4627.4	4461.2	3.8
K	-10.4	-3465.6	3329.4	4.3
Rb	-11.4	-3254.9	3119.7	4.5
Cs	-10.8	-3013.4	2980.8	4.8

TABLE I. Solvation energies of Ak atoms and ions, sinking energy of the Ak^+ ion, and radius of the first solvation shell corresponding to the $^4He_{2000}$ droplet; see Eqs. (7-8) and related text for definitions.

atom resides is clearly visible. From the Ak-He pair potentials drawn in Fig. 2 (bottom insert), it can be noticed that the stronger the Ak-He interaction and the shorter its equilibrium distance, the deeper the dimple and the closer the Ak atom to the distorted droplet surface. This was also the case in the ^{4}He-DFT study of $Ak@He_{1000}$ absorption spectra (see Ref. 10 and Table I in Ref. 28).

Upon ionization, the Ak^+ ion sinks towards its equilibrium position at the center of the droplet. The spherically averaged density profile of $Ak^+@^4He_{2000}$ complexes at equilibrium is shown in the top panel of Fig. 2 as a function of the distance to the cation. The bottom panel of Fig. 2 shows the Ak^+-He pair potentials.[23] The neutral Ak-He pair potentials[22] are also displayed as an insert. It can be seen from these figures that the effect of the impurity (Ak or Ak^+) on the He droplet, even if sizeable, remains local.

A well-defined inner (solvation) shell of He atoms around the Ak^+ cation can be clearly seen in the insert in the top panel of Fig. 2, showing a focus on the helium density around the cation ($r \leq 10$ Å); see also Refs. 5 and 29. Note also that for a large drop such as $^4He_{2000}$, two additional shells are distinguishable. However, the concept of shell is rather approximate in this case since, in contrast with the first solva-

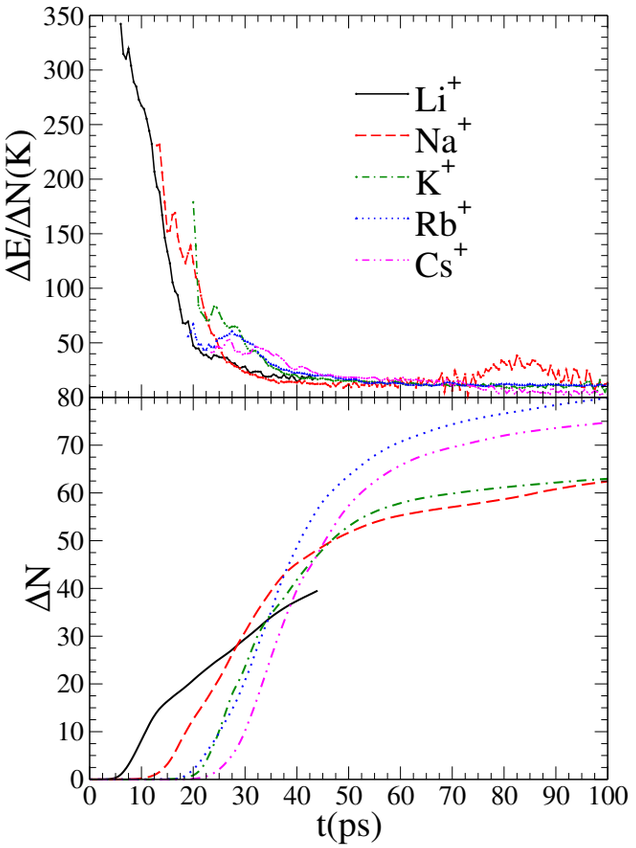

FIG. 3. Droplet relaxation by helium atom ejection during the sinking dynamics of $Ak^+@^4He_{2000}$. Top plot: Time evolution of the average energy dissipated per ejected atom, $\Delta E/\Delta N$ (see text for definition). Bottom plot: Number ΔN of ejected He atoms as a function of time.

tion shell which is well separated from the others, the helium density in between shells is significant. The average density in the first shell is well-above the freezing density of bulk liquid ^{4}He (0.026 Å^{-3}). Although this might be considered as an indication of a helium solid-like structure in the first solvation shell, to clearly assess the solid-like or liquid-like character of the structure around the cation, one should also consider the dynamical behavior of the helium atoms. This is beyond the capabilities of the ^{4}He-DFT approach, but could be addressed by more fundamental methods such as path integral Monte Carlo (PIMC).[30,31]

As will be discussed below, density functional calculations of ^{4}He samples hosting very attractive impurities such as cations yield very structured helium densities displaying high density "blobs" in the vicinity of the cation; depending on the impurity, these blobs have a clearly identifiable symmetry: e.g., icosahedral for the case of Be^+.[29] Although one might be tempted to interpret these blobs as representing actual helium atoms, it should be kept in mind that what ^{4}He-DFT yields is the helium density $\rho(\mathbf{r})$, i.e., the squared order parameter $|\Psi(\mathbf{r})|^2$. It would be misleading to associate a helium atom to each blob in the structure. However, to the extent that these density blobs are separated by quasi zero helium density regions, they can be taken as an indication that the corresponding shell is quasi-rigid, i.e., solid-like.

Several quantities of interest can be obtained from the static ^{4}He-DFT calculations. In particular, the energy available in the sinking process, i.e., the difference between the initial total energy at the ionization time and the one at $Ak^+@^4He_N$ equilibrium:

$$E_{sink}(Ak^+@^4He_N) = E_{dim}(Ak^+@^4He_N) - E_{bulk}(Ak^+@^4He_N)\,, \tag{7}$$

where E_{dim} is the energy of the initial $Ak^+@^4He_N$ complex where the ion just replaced the neutral atom at the dimple position, and E_{bulk} is the energy of the relaxed $Ak^+@^4He_N$ system. These energies are collected in Table I for all Ak cations and $N = 2000$. They are very high, increasing from 2981 K for Cs^+ to 7008 K for Li^+. This shows that ion sinking is a very energetic process, which will generate strong excitations in the helium droplet. Another relevant quantity, also collected in Table I, is the solvation energy S_X of the Ak atoms and of the Ak^+ ions into a ^4He_N droplet defined as

$$S_X = E(X@^4He_N) - E(^4He_N)\,. \tag{8}$$

All these quantities depend on N and on the functional used to obtain them, so minor differences may be found with former published values. As an illustration of the size dependence, we have obtained $S_{Na} = -10.4$ K, $S_{Na^+} = -4673.5$ K, and $E_{sink} = 4496.2$ K for a $Na^+@^4He_{5000}$ droplet, to be compared to the values in Table I for $N = 2000$. We have also calculated the value of S_{Na} for the free surface of superfluid helium, which corresponds to the asymptotic $N \to \infty$ limit: $S_{Na} = -10.7$ K.

Also shown in Table I is the radius of the first solvation shell, r_1, defined as the location of the first minimum of the density profile when the cation is at the droplet center. It is used to compute the He atoms content n_1 of the first (spherically averaged) solvation shell by integrating the He density profile from the location of the Ak^+ ion equilibrium position, $r = 0$, to $r = r_1$.

An extensive compilation of the size of snowballs and other energetically favorable structures around a wide variety of ions can be found in Tables 1 and 2 of Ref. 4. Table II here compares the values for Ak^+ cations obtained in the present work with the ones calculated by different authors using other approaches: These may refer to anomalies in computed dissociation energies, or to sizes at which radial distribution functions or other measures indicate closure of a solvation shell.[4] As can be seen in Table II, ^{4}He-DFT tends to overestimate the number of ^{4}He atoms in the first solvation shell.

Let us comment some of the results displayed in Table II. The helium-Ak^+ interaction is usually taken as a sum of pairwise potentials.[5,30,32–40] The attractive part of this two-body (2B) interaction is dominated by the interaction between the ion charge and the induced dipole in the He atom, $V_{qd}(r) = -q^2\alpha_{He}/(2r^4)$ (in atomic units), q being the ion charge and α_{He} the He atom polarizability. However, several studies[41–44] have also taken into account non pairwise additive interactions –denoted here as three-body (3B) contributions– arising from

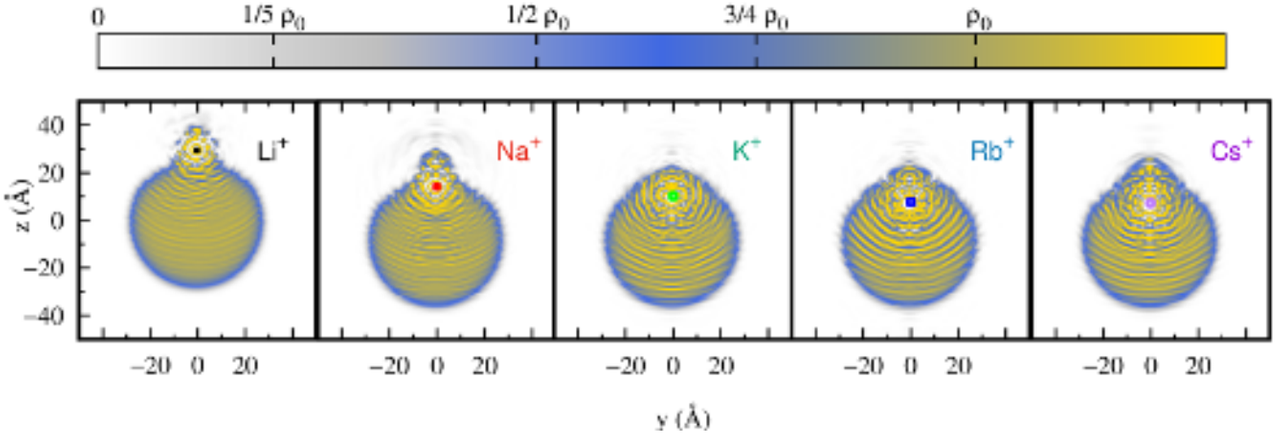

FIG. 4. Ion location and helium density (two-dimensional cut in a symmetry plane) after $t = 20$ ps of Ak^+ sinking in a $^4He_{2000}$ nanodroplet. The density scale on top is given in units of ρ_0, the bulk superfluid density at zero temperature and pressure ($\rho_0 = 0.0218$ Å^{-3}). Individual movies presenting the time evolution of the 2D cuts side by side with that of the spherically averaged density profile (see Fig. 5) are presented as Supplementary Material for each Ak^+.

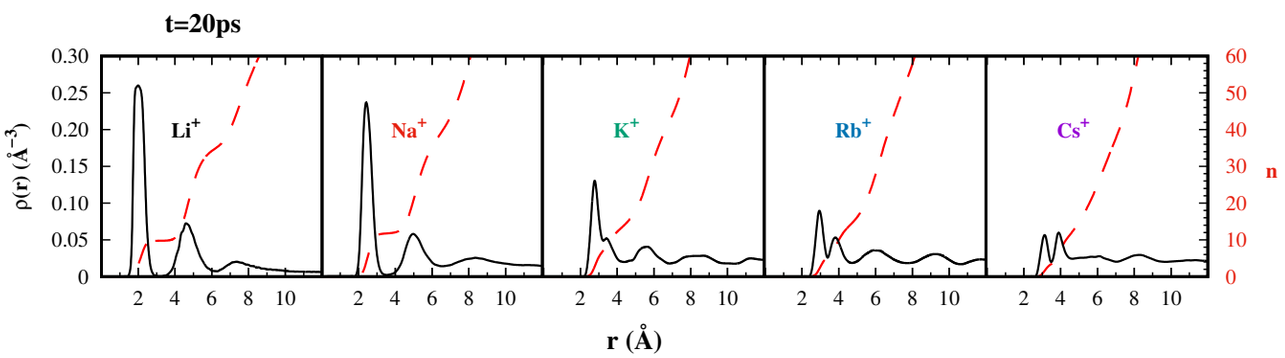

FIG. 5. Spherically averaged density profile (black solid line, left vertical scale) and number of He atoms $n(r)$ as a function of the distance to the ion (red dashed line, right vertical scale) after $t = 20$ ps of Ak^+ sinking in a $^4He_{2000}$ nanodroplet. Individual movies presenting the time evolution of the spherically averaged density profile side by side with that of 2D cuts (see Fig. 4) are presented as Supplementary Material for each Ak^+.

induced dipoles interacting between themselves. It has been argued[41] that these 3B interactions could be responsible for the overestimation of the size of the Na^+ first solvation shell by simulations including only 2B interactions compared to the experimental results of An der Lan et al.[11] This claim is disputed by other theorists. While it is acknowledged that including 3B effects usually decreases the binding energy of the system and, consequently, the evaporation energies, it has been found that it does not alter the general picture, i.e., the relative stability of the configurations appears to be unchanged.[42,43] In particular, the first shell closure was found at the same number of helium atoms (see e.g. Fig. 7 of Ref. 42 for Li^+ and Fig. 4 left of Ref. 43 for Pb^{2+}). It was also concluded[44] that the structural observables are essentially unaffected by 3B corrections and therefore the results on cluster structuring evolution remained reliable when one only uses the 2B potential.

An interesting point discussed by Galli et al.[32] is the influence of Bose statistics on the structure of $X^+@He_N$ systems. They have compared PIMC simulations of doped droplets with or without sampling permutations between ^{4}He atoms in the $X^+@^4He_{64}$ system with X= Na or Mg. While the effect of bosonic exchange on energies was found to be significant, the density profile around Na^+ and Mg^+ remained unaffected (see Fig. 3 in that reference), and not only in the first solvation shell where it might have been expected due to its solid-like character. It is worth mentioning that boson exchanges are not considered in the PIMC calculations of Ref. 41, and that when only 2B interactions are considered, they find the same size for the first solvation shell of Na^+ as the PIMC calculations which include them.[32] Unfortunately, we cannot determine the relative importance of 3B and permutation statistics effects on the energetics and morphology of these systems from the published results.

Two different strategies are usually applied by theoreticians to determine the size of snowballs: either simulate ionic systems with a number of ^{4}He atoms substantially larger than the

	PIMC	PIGSMC[30]	SWF-VMC	DMC[33]	DFT	Class.-sim.[36]	BH-DMC/PIMC
Li^+		8.2		6, 10	$12^{(p.w.)}$		4, 6, 8[42]; 5, 6, 8, 10^{44}
Na^+	12^{32};16^{34}; 10^{41}	12	9^{38}; 12^{35}		$14^{14;(p.w.)}$		12^{44}
K^+	15^{32}		12^{38}; 15^{35}		$17^{(p.w.)}$	15	15^{44}
Rb^+					19^5; $18^{(p.w.)}$		
Cs^+	18^{32}		17.5^{35}		$21^{5;(p.w.)}$		12, 17^{37}

TABLE II. Number of He atoms in the first solvation shell n_1 and of other energetically favorable structures around Ak^+ ions obtained with different *static* theoretical approaches in the indicated references (p.w.: present work). PIMC, path integral Monte Carlo; PIGSMC, path integral ground-state Monte Carlo; SWF-VMC, shadow wave function variational Monte Carlo; DMC, diffusion Monte Carlo; DFT, ^{4}He-DFT; Class-sim., classical simulation method; BH-DMC/PIMC, basin-hopping DMC/PIMC.

snowball[30,32] and deduce snowball sizes from integrated densities, or add ^{4}He atoms "one by one" to the ion[36,41–43] and deduce them from the relative stability of the Ak^+-He_n complexes. For some Ak^+, a number of the latter calculations have been stopped before reaching the first solvation shell closure.[39,40]

The ^{4}He-DFT method used in this work pertains to the first strategy. In order to compare with the second one, we have also carried out static calculations for $Na^+@^4He_n$ complexes, $n = 2$ to 16. The resulting total energies $E_n = E(Ak^+@^4He_n)$ are collected in Table III, together with the dissociation (or evaporation) energies D_n and second energy differences $\Delta_2(n)$ defined as

$$D_n = E_{n-1} - E_n\,, \tag{9}$$

$$\Delta_2(n) = D_n - D_{n+1} = E_{n+1} - 2E_n + E_{n-1}\,. \tag{10}$$

Local maxima of $\Delta_2(n)$ are expected to characterize the most stable configurations, some of them corresponding to solvation shell closures. The results in Table III illustrate the difficulties in using a single criterion for determining the closure of the first solvation shell. The maximum of the second energy difference Δ_2 points to $n_1 = 12-13$ as the maximum number of He atoms in the first solvation shell, with a strong decrease for $n = 14$ down to a very small Δ_2 value for $n = 15$. At variance, direct integration of the spherically averaged density up to r_1 yields $n_1 = 14$, as in Ref. 14. Hence the two criteria (energetics and density integration) fairly agree but not necessarily coincide.

Table II also reveals that no structure is particularly stable below n_1 within the ^{4}He-DFT approach. This is due to the fluid-like character of the ^{4}He-DFT description of the system. Yet, a plot of Δ_2 *vs.* n exhibits some anomalies around $n = 4-5$ and around $n = 7-8$, indicating that energetically favorable structures might show up around these n values. Atomic resolved calculations, such as the ones referred to above, are inherently well suited to handle these structures and determine the most stable complexes. Experimentally they can be determined as local anomalies in the Ak^+He_n ion yields in mass spectrometry experiments.[11]

n	E_n (K)	D_n (K)	Δ_2 (K)
2	-648.49		
3	-972.64	324.2	1.9
4	-1294.92	322.3	8.4
5	-1612.56	317.6	8.4
6	-1921.77	309.2	13.4
7	-2217.55	295.8	21.2
8	-2492.14	274.6	23.8
9	-2742.92	250.8	32.4
10	-2961.35	218.4	38.3
11	-3141.45	180.1	42.2
12	-3279.34	137.9	44.0
13	-3373.23	93.9	43.6
14	-3423.51	50.3	24.1
15	-3449.73	26.2	1.1
16	-3474.87	25.1	

TABLE III. Total energy E_n, dissociation energy D_n, and second energy difference Δ_2 of some $Na^+@^4He_n$ complexes; see Eqs. (9-10) and related text.

	$t_{sim}(ps)$	ΔN	A (ps^{-1})
Li^+	44	40	[1.46, 1.46]
Na^+	100.8	63	[0.79, 0.74]
K^+	100.8	63	[0.67, 0.50]
Rb^+	100.8	80	[0.81, 0.61]
Cs^+	100.8	75	[0.74, 0.67]

TABLE IV. Number of emitted He atoms ΔN and average energy per emitted He atom $\Delta E/\Delta N$ for the duration t_{sim} of the dynamics simulation of Ak^+ ions sinking in a $^4He_{2000}$ droplet. Also given is the slope of the $n(t) = At$ law, see text for explanation.

B. Dynamics

The sinking dynamics is triggered by substituting the Ak-He pair potential with that of the Ak^+-He pair in the $Ak@^4He_{2000}$ equilibrium configuration of Fig. 1.[5] The simulations then proceeded as explained in Sec. II, and were conducted for about t_{sim}=100 ps, see Table IV. Note that the simulation time is shorter for Li^+ than for the other ions. The much stronger He-Li^+ attraction (the He-Li^+ well depth is more than double the one of the next largest well depth, that of He-Na^+, see Fig. 2), combined with the light mass of the

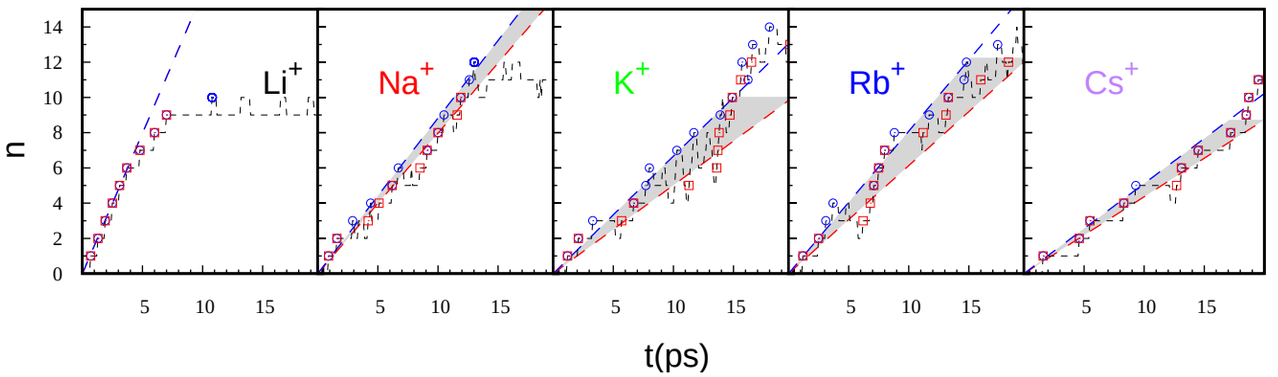

FIG. 6. Number of He atoms n around the Ak^+ ions as a function of t for $Ak^+@^4He_{2000}$. Open blue circles correspond to the first time at which the number of He atoms is equal to the integer value n, where as open red squares mark the first time it reaches n with no more fluctuations back to $(n-1)$. The lines are the best linear fits $n(t) = At$ (a hint pointing to a Poissonian capture process) for the $Ak^+@He_n$ complexes up to $n = 5$ for each definition. The shadowed regions between the two lines give an idea of the uncertainty on the rates obtained within the ^{4}He-TDDFT approach. See text for more details.

cation, required a much smaller time step for the dynamics which could not be run for much longer times within reasonable computing time cost. Yet, the simulation time is long enough to observe its sinking.

As mentioned in Sect. III A, the available energy during the sinking process (E_{sink} in Table I), is very high . Therefore, extensive helium atom ejection (the only energy dissipation mechanism by the droplet in our approach), is expected. The number of ejected atoms ΔN as well as the average dissipated energy per ejected atom $\Delta E/\Delta N$ are calculated as a function of time as follows

$$\begin{aligned} \Delta N(t) &= N - \langle |\Psi(\mathbf{r},t)|^2 \rangle \\ \frac{\Delta E}{\Delta N} &= -\frac{(\Delta E/\Delta t)}{(\Delta N/\Delta t)} \end{aligned} \tag{11}$$

They are represented in Fig. 3 for all alkali ions. The time interval Δt was set at 0.5 ps and a 3-point formula was used to calculate $\Delta E/\Delta t$ and $\Delta N/\Delta t$ in order to minimize unavoidable fluctuations. The $\Delta E/\Delta N$ curves start at the time at which about one atom has been emitted. It is worth noting that because of the way $\Delta N(t)$ is calculated (by subtracting the integrated helium density remaining in the simulation box from the initial number of atoms, first Eq. (11)), emitted helium atoms (or rather, density) are only accounted for when they reach the absorption buffer of the box, which inevitably adds a delay. The numbers of emitted He atoms ΔN at the end of each simulation are collected in Table IV.

As can be seen in Fig. 3, the time evolution of the number of emitted atoms follows the same behavior for all alkalis: first a fast increase after a variable time delay, and then a slower increase. Also, despite the large differences in He-Ak^+ interactions (well depth V_{min} and equilibrium distance $R_{V_{min}}$, see insert in Fig. 2), the time evolution of $\Delta E/\Delta N$ is remarkably similar for all alkalis. The first emitted atoms, $t \lesssim 20$ ps, have a rather high kinetic energy, up to 300-350 K for Li^+ in the first 10 ps. This is much higher than the 7 K corresponding approximately to the extraction energy of one helium atom in bulk liquid helium in thermodynamic equilibrium a zero temperature and pressure. These highly energetic and promptly emitted atoms constitute a significant proportion of the emitted helium atoms. This shows that estimating the number of emitted atoms by dividing the overall excitation energy by 7 K can give a very rough result: promptly emitted helium atoms can be, and usually are, very energetic. The energy dissipated per atom then slowly decreases to about 10 K or below for $40 \lesssim t \lesssim 100$ ps. This common asymptotic behavior is expected since it is close to the helium atom evaporation regime where each atom dissipates the equivalent of its binding energy to the droplet, about 7 K. It is remarkable that an evaporation-like regime can be attained in several tens of picoseconds, given the amount of energy initially present in the system. The only notable difference between alkalis is the value of $\Delta E/\Delta N$ at the beginning of the solvation dynamics, and the time it takes for the equivalent of the first atom to be emitted. The lighter alkalis, especially Li^+, give raise to very energetic helium atoms which appear earlier, presumably because they are faster in reaching the absorption buffer of the simulation box where they are detected.

Finally, there is a peculiar oscillation between 75 and 90 ps for Na^+. Examination of the movies introduced in the next paragraph shows that this oscillation coincides with the eruption of energetic helium atoms on the opposite side of the sinking: this usually results from the creation of a travelling surface wave at the sinking point which propagates on the droplet surface until collapsing at the opposite point from its creation, then producing a helium atoms burst.

Movies illustrating the sinking dynamics for each Ak^+ cation are provided in the supplementary material. Two panels are displayed. The one on the left hand side shows the time evolution of the ion position inside the helium droplet, represented as a two-dimensional (2D) cut of the density in a symmetry plane. The one on the right hand side depicts the time evolution of the spherically averaged helium density profile around Ak^+ as a function of the distance r to the cation. The latter movie is particularly appealing as it shows the dy-

namical formation of the solvation shells and their contents.

The snapshots corresponding to $t = 20$ ps are shown in Fig. 4 (Ak^+ position in a 2D-cut through the helium density) and Fig. 5 (spherically averaged density profile around Ak^+). At that time, the first solvation shell is already well in place for the lighter alkalis (Li^+, Na^+), but not for the heavier ones (K^+, Rb^+ and Cs^+), as can be seen by the separation of the first density peak from the rest of the spherically averaged density. This is remarkable, since as can be seen in Fig. 4, the ions are already well within the bulk of the droplet. This difference is presumably due to the much deeper He-Li^+ and He-Na^+ interaction potential well.

As can be seen from the movies, the droplets are still rather excited at the end of the simulations. They are far from their final equilibrium configuration, which corresponds to an Ak^+ ion at rest at the center of the remaining ^4He_M spherical droplet (with $M < 2000$). A sizeable part of the excitation energy remains in the droplet in the form of density waves and large amplitude surface modes, plus some kinetic energy in the ion and in the droplet itself. The absence of viscosity implies that the excitation energy can only be dissipated by atom evaporation.

C. Comparison with experiment

In the experiment by Albrechtsen et al. recalled in the Introduction,[14] the first step consists in ionizing the Ak atom attached to a helium droplet doped with a xenon atom. In the work presented here, there is no xenon atom at the droplet center. However, due to the droplet size, the interaction of the sinking Ak^+ ion with a neutral impurity residing in the bulk of the droplet is very small during the first picoseconds of the pump process and can be neglected. Hence our simulations sensibly represent the pump process. Even though we have not yet conducted the more demanding simulation of the whole pump-probe process, the comparison of the ion solvation rate $n(t)$ reported in Fig. 6 and Table IV with experimental results should already be meaningful, at least at short times.

Due to the strong Ak^+-He interaction, the first n He atoms attached to the ion during the first stages of the sinking process are expected to remain tightly bound to it during the Coulomb repulsion process and lead to the detection of $Ak^+@^4He_n$, as explicitly shown in the Na^+ case.[14] Within the ^{4}He-DFT approach, this number has been obtained by integrating the helium spherically averaged density profile inside the first solvation sphere of radius r_1 around the Ak^+ ion. Fig. 6 displays the time-dependence of n for all alkalis. This number sometimes fluctuates back and forth by ± 1 with time. Open blue circles correspond to the first time at which an integer number of atoms $n = 1, 2, 3, \ldots$ is attached to the cation. Open red squares correspond to the time starting from which this number no longer fluctuates back to $n-1$. As can be seen from Fig. 6, the time-dependence of n is linear during the first picoseconds, pointing to a Poissonian capture process in which the helium atoms bind independently of each other and with a constant rate.[14] This is especially true for the more attractive Li^+ and Na^+ cations.

For each alkali ion, we have fitted $n(t)$ to a linear form $n(t) = At$ for n up to 5; the parameter A can be identified with the binding rate. Each fit was performed twice, once for each definition of $n(t)$ discussed in the preceding paragraph, the first definition (first time the integrated density in the solvation sphere reaches n) yielding a larger value of A than the second one (first time it reaches n with no more fluctuations back to $n-1$). Both A values are reported in between brackets in Table IV and plotted as straight, dashed lines in Fig. 6 (blue or red for the first or second definition, respectively). The shadowed regions between the two lines in the panels of Fig. 6 give an idea of the uncertainty on the rates obtained within the ^{4}He-TDDFT approach. Table IV shows that the binding rate A is very similar for all alkalis, except for Li^+ for which it is much larger. This is due to the combination of two effects, namely, a deeper dimple for neutral Li together with a stronger Li^+-He attraction.

We have found that the number of He atoms in the first solvation shell at the end of the simulation is smaller than the one obtained from the static calculation for both lighter alkalis: 9 instead of 12 for Li^+ and 12 instead of 14 for Na^+. For the heavier alkalis, it is equal (17 for K^+, 18 for Rb^+ and 21 for Cs^+). The reason why this occurs for the lighter alkalis and not for the heavier ones is unclear. It could be due to the fact that the first solvation shell is more rigid for the lighter alkalis, as can be seen by scrutinizing the density profiles at the end of the dynamics: the helium density does not go quite to zero between the first and the second solvation shell for the heavier alkalis. This is also true for the equilibrium structures shown in Fig. 2. This allows for continuous equilibration of the density between the first and the second shell. In contrast, the two shells are clearly separated in the equilibrium structure of the lighter alkali ions, and the isolation of the first density shells occurs before the end of the dynamics, around 20 ps for Li^+ and 25-30 ps for Na^+. After that the integrated density (or number of helium atoms) inside the first solvation shells no longer varies.

IV. SUMMARY AND OUTLOOK

We have described the sinking of alkali ions Ak^+ in a He droplet containing 2000 atoms using the ^{4}He-TDDFT approach. The movies in the supplementary material as well as the energetics of the process (excitation energy) show that this corresponds to a rather violent dynamics for the droplet. This is confirmed by the high energy dissipated per ejected helium atom, especially in the first 10-20 ps. The time evolution of the droplet energy relaxation by helium atom emission is found to be remarkably similar between all alkalis, the most notable difference being the amount of energy dissipated per helium atom at the beginning of the dynamics, which is highest for the lightest alkali ions, Li^+, followed by Na^+, following the strength of decreasing He-Ak^+ interaction. The first emitted helium atoms also appear earlier for Li^+, which makes sense since they are also faster.

In order to relate our findings to the first experiment de-

signed to unravel the primary steps of ion solvation in helium nanodroplets,[14] we have determined the number of He atoms in the first solvation shell as a function of time. Our simulations show how these shells are dynamically built around the cation. The number of helium atoms inside the first solvation shell are found to linearly increase with time during the first stages of the process, in agreement with the linear behavior observed in the experiment on Na^+,[14] pointing to a Poissonian capture process.

Remarkably, we have found that the number of helium atoms in the first solvation shell is lower at the end of the (limited) dynamics than obtained at equilibrium for Li^+ and Na^+. This points to kinetic rather than thermodynamical control of the snowball size for small and strongly attractive ions.

The more demanding simulations of the full pump-probe processes are under progress.

V. SUPPLEMENTARY MATERIAL

We provide as supplementary material one movie for each alkali ion, $Ak^+ \equiv Li^+$, Na^+, K^+, Rb^+, and Cs^+, illustrating the real-time simulations of the sinking of Ak^+ ions addressed in this work. This multimedia material helps capture physical details that would be difficult to present and thoroughly describe in the main text. Two panels are displayed in each movie. The one on the left hand side shows the time evolution of the ion position inside the helium droplet, represented as a two-dimensional (2D) cut of the density in a symmetry plane, as shown in the snapshots of Fig. 4. The one on the right hand side depicts the time evolution of the spherically averaged helium density profile around Ak^+ as a function of the distance r to the cation, as shown in the snapshots of Fig. 5. It is particularly appealing as it shows the dynamical formation of the solvation shells and their contents.

ACKNOWLEDGMENTS

A computer grant from CALMIP high performance computer center (grant P1039) is gratefully acknowledged. This work has been performed under Grant No. PID2020-114626GB-I00 from the MICIN/AEI/10.13039/501100011033 and benefitted from COST Action CA21101 "Confined molecular systems: form a new generation of materials to the stars" (COSY) supported by COST (European Cooperation in Science and Technology).

AUTHOR DECLARATIONS

Conflict of Interest

The authors have no conflicts to disclose.

DATA AVAILABILITY

The data that support the findings of this study are available from the corresponding author upon reasonable request

[1] B. Tabbert, H. Günther, and G. zu Putlitz, J. Low Temp. Phys. **109**, 653 (1997).
[2] S. L. Fiedler, D. Mateo, T. Aleksanyan, and J. Eloranta, Phys. Rev. B **86**, 144522 (2012).
[3] W. Wei, Z. Xie, L. N. Cooper, G. M. Seidel, and H. J. Maris, J. Low Temp. Phys. **178**, 78 (2015).
[4] T. González-Lezana, O. Echt, M. Gatchell, M. Bartolomei, J. Campos-Martínez, and P. Scheier, Int. Rev. Phys. Chem. **39**, 465 (2020).
[5] A. Leal, D. Mateo, A. Hernando, M. Pi, M. Barranco, A. Ponti, F. Cargnoni, and M. Drabbels, Phys. Rev. B **90**, 224518 (2014).
[6] D. Mateo, A. Leal, A. Hernando, M. Barranco, M. Pi, F. Cargnoni, M. Mella, X. Zhang, and M. Drabbels, J. Chem. Phys. **140**, 131101 (2014).
[7] X. Zhang and M. Drabbels, J. Chem. Phys. **137**, 051102 (2012).
[8] S. Müller, M. Mudrich, and F. Stienkemeier, J. Chem. Phys. **131**, 044319 (2009).
[9] J. Tiggesbäumker and F. Stienkemeier, Phys. Chem. Chem. Phys. **9**, 4748 (2007).
[10] O. Bürmann, G. Droppelmann, A. Hernando, R. Mayol, and F. Stienkemeier, J. Phys. Chem. A **111**, 12684 (2007).
[11] L. An der Lan, P. Bartl, C. Leidlmair, R. Jochum, S. Denifl, O. Echt, and P. Scheier, Chem. Eur. J. **18**, 4411 (2012).
[12] M. Theisen, F. Lackner, and W. E. Ernst, Phys. Chem. Chem. Phys. **12**, 14861 (2010).
[13] M. Theisen, F. Lackner, and W. E. Ernst, J. Chem. Phys. **135**, 14861 (2011).
[14] S. H. Albrechtsen, C. A. Schouder, A. Viñas-Muñoz, J. K. Christensen, C. E. Petersen, M. Pi, M. Barranco, and H. Stapelfeldt, Nature **623**, 319 (2023).
[15] Y. Markus, *Ions in solution and their solvation*, ch. 4, p. 107 (Whiley 2015).
[16] F. Ancilotto, M. Barranco, F. Coppens, J. Eloranta, N. Halberstadt, A. Hernando, D. Mateo, and M. Pi, Int. Rev. Phys. Chem. **36**, 621 (2017).
[17] M. Pi, F. Ancilotto, F. Coppens, N. Halberstadt, A. Hernando, A. Leal, D. Mateo, R. Mayol, and M. Barranco, *4He-DFT BCN-TLS: A Computer Package for Simulating Structural Properties and Dynamics of Doped Liquid Helium-4 Systems*. `https://github.com/bcntls2016/`
[18] F. Dalfovo, A. Lastri, L. Pricaupenko, S. Stringari, and J. Treiner, Phys. Rev. B **52**, 1193 (1995).
[19] M. Barranco, R. Guardiola, S. Hernández, R. Mayol, J. Navarro, and M. Pi, J. Low Temp. Phys. **142**, 1 (2006).
[20] M. Barranco, F. Coppens, N. Halberstadt, A. Hernando, A. Leal, D. Mateo, R. Mayol, and M. Pi, *Zero temperature DFT and TDDFT for ^{4}He: A short guide for practitioners.* `https://github.com/bcntls2016/DFT-Guide/blob/master/dft-guide.pdf`
[21] F. Ancilotto, M. Barranco, F. Caupin, R. Mayol, and M. Pi, Phys. Rev. B **72**, 214522 (2005).
[22] S. H. Patil, J. Chem. Phys. **94**, 8089 (1991).
[23] A. D. Koutselos, E. A. Mason, and L. A. Viehland, J. Chem. Phys. **93**, 7125 (1990).
[24] M. Frigo and S. G. Johnson, Proc. IEEE **93**, 216 (2005).
[25] F. Coppens, F. Ancilotto, M. Barranco, N. Halberstadt, and M. Pi, Phys. Chem. Chem. Phys. **21**, 17423 (2019).
[26] A. Ralston and H. S. Wilf, *Mathematical methods for digital computers* (John Wiley and Sons, New York, 1960).
[27] D. Mateo, D. Jin, M. Barranco, and M. Pi, J. Chem. Phys. **134**, 044507 (2011).
[28] E. García-Alfonso, F. Coppens, M. Barranco, M. Pi, F. Stienkemeier and N. Halberstadt, J. Chem. Phys. **152**, 194109 (2020).
[29] F. Ancilotto, M. Pi, R. Mayol, M. Barranco, and K. K. Lehmann, J. Phys. Chem. A **111**, 12695 (2007).
[30] S. Paolini, F. Ancilotto, and F. Toigo, J. Chem. Phys. **126**, 124317 (2007).
[31] F. Brieuc, C. Schran, and D. Marx, Phys. Rev. Res. **5**, 043083 (2023).
[32] D. E. Galli, D. M. Ceperley, and L. Reatto, J. Phys. Chem. A **115**, 7300 (2011).
[33] C. Di Paola, F. Sebastianelli, E. Bodo, I. Baccarelli, and F. A. Gianturco, J. Chem. Theory Comput. **1**, 1045 (2005).

[34]A. Nakayama and K. Yamashita, J. Chem. Phys. **112**, 10966 (2000).
[35]M. Rossi, M. Verona, D. E. Galli, and L. Reatto, Phys. Rev. B **69**, 212510 (2004).
[36]E. Yurtsever, E. Yildirim, M. Yurtsever, E. Bodo, and F. A. Gianturco, Eur. Phys. J. D **43**, 105 (2007).
[37]R. Pérez de Tudela, P. Martini, M. Goulart, P. Scheier, F. Pirani, J. Hernández-Rojas, J. Bretón, J. Ortiz de Zárate, M. Bartolomei, T. González-Lezana, M. I. Hernández, J. Campos-Martínez, and P. Villarreal, J. Chem. Phys. **150**, 154304 (2019).
[38]D. E. Galli, M. Buzzacchi, and L. Reatto, J. Chem. Phys. **115**, 10239 (2001).
[39]F. Sebastianelli, E. Bodo, I. Baccarelli, C. Di Paola, F. A. Gianturco, and M. Yurtsever, Computational Materials Science **35**, 261 (2006).
[40]E. Coccia, E. Bodo, F. Martinetti, F. A. Gianturco, E. Yildrim, M. Yurtsever, and E. Yurtsever, J. Chem. Phys. **126**, 124319 (2007).
[41]N. Issaoui, A. Kawther, H. Ghalla, S. J. Yaghmour, F. Calvo, and B. Ouija, J. Chem. Phys. **141**, 174316 (2014).
[42]M. Rastogi, C. Leidlmair, L. An der Lan, J. Ortiz de Zárate R. Pérez de Tudela, M. Bartolomei, M. I. Hernández, J. Campos-Martínez, T. González-Lezana, J. Hernández-Rojas, J. Bretón, P. Scheier, and M. Gatchell, Phys. Chem. Chem. Phys. **20**, 25569 (2018).
[43]P. Slavíček and M. Lewerenz, Phys. Chem. Chem. Phys. **12**, 1152 (2010).
[44]F. Marinetti, E. Coccia, E. Bodo, F. A. Gianturco, E. Yurtsever, M. Yurtsever, and E. Yildirim, Theor. Chem. Acc. **118**, 53 (2007).